DOI: 10.1021/ma901891b

Macromolecules
ARTICLE

Symmetry Transition in Thin Films of Diblock Copolymer/Homopolymer Blends

Vindhya Mishra,[†] Su-mi Hur,[†] Eric W. Cochran,[‡,∥] Gila E. Stein,[§,⊥] Glenn H. Fredrickson,[†] and Edward J. Kramer*,[†]

[†]*Department of Chemical Engineering and Department of Materials, University of California, Santa Barbara, California 93106,* [‡]*Department of Chemical and Biological Engineering, Iowa State University, Iowa 50011, and* [§]*Department of Chemical and Biomolecular Engineering, University of Houston, Houston, Texas 77204.* [∥] *Previous address: University of California, Santa Barbara.* [⊥] *Previous address: University of California, Santa Barbara.*

Received August 25, 2009; Revised Manuscript Received December 23, 2009

ABSTRACT: The effect of blending small weight fractions of low molecular weight majority block homopolymer on the structure of multilayer films of spherical morphology poly(styrene-*b*-2vinylpyridine) [PS−P2VP] has been studied. The structure of the films was characterized with grazing-incidence small-angle X-ray scattering (GISAXS) and transmission electron microscopy (TEM). In multilayer films of PS−P2VP, competition between hexagonal packing of the spherical domains preferred at the surfaces with the BCC (110) packing preferred by the internal layers leads to a transition in the packing symmetry as the number of sphere layers (n) is increased.[1] Neat PS−P2VP exhibits hexagonal close-packed (HCP) symmetry up through $n = 4$, but at four layers coexistence of hexagonal and face-centered orthorhombic phases is observed. At $n = n^* = 5$ the face-centered orthorhombic structure (FCO) is the stable phase. On increasing n further, the FCO phase continuously distorts to approach the arrangement of the BCC (110) plane. We observe that blending a small weight fraction of low molecular weight PS homopolymer with PS−P2VP suppresses this transition and stabilizes the hexagonal close-packed arrangement beyond four layers. Moreover, n^* increases with increasing weight fraction of incorporated homopolymer for the small weight fractions of homopolymer used in this study. Self-consistent-field theory simulations designed to mimic the experimental system corroborate that n^* is expected to increase and show that the PS homopolymer segregates to the interstices of the HCP unit cell. This suggests that the homopolymer reduces the stretching of the PS block and the free energy penalty of HCP relative to BCC inner layers. This result is consistent with the hypothesis that the excessive stretching requirement in an HCP arrangement is the cause of its higher free energy as compared to the BCC lattice.

Introduction

As a result of a large number of theoretical and experimental studies, the bulk phase behavior for linear diblock copolymers has been well mapped out.[2−7] However, newer technological applications for block copolymers (as templates for nanopatterning[8−10] or as nanoporous membranes[11,12]) necessitate using the polymer in "resist-like" thin films so that they can be easily integrated into existing methods for fabrication. Confining the block copolymer to a thin film adds another degree of geometric frustration to the system as well as increases the relative contribution of surface effects. As a result of this, the equilibrium behavior of block copolymers in thin films can be very different from the bulk. Barring a few cases,[13−15] however, the differences have not been systematically studied. In order to draw any universal conclusions relevant for all thin film cases, it will be useful to first identify those contributions to the free energy that arise in thin films that may lead to differences in equilibrium behavior compared to the bulk case.

Spherical morphology diblock copolymers are an ideal system for such an investigation. It has been shown both experimentally[1] and theoretically[16] that sphere-forming diblock copolymer adopts a hexagonal arrangement in the case of monolayers and a BCC arrangement for bulk systems. Hence, as the film thickness is increased in a controlled manner, the equilibrium arrangement of the spheres is expected to change. This transition has been confirmed experimentally by Stein and co-workers for a system that consists of poly(styrene-*b*-2-vinylpyridine) [PS−P2VP] diblock copolymers that form spheres of P2VP in PS surroundings.[1] In bulk the P2VP microdomains are arranged in a body-centered cubic (BCC) lattice, as expected. However, on decreasing the film thickness to below 15 sphere layers, the symmetry transitions to a face-centered orthorhombic (FCO) phase, and below four layers of spheres, the arrangement is hexagonal close-packed (HCP). The preferred arrangement of the spheres is driven by the tendency to minimize packing frustration while maintaining constant monomer density. A major contribution to the packing frustration comes from the stretching of the majority block to fill the interstices.[17,18] Theoretical work has shown that in three dimensions, compared to a close-packed arrangement, the BCC lattice requires less stretching of the majority block to fill the interstitial space and maintain uniform monomer density.[16,19,2] Although the lower stretching requirement may be the reason the BCC is preferred in the bulk phase as opposed to a close-packed arrangement, there has been no experimental test of this theoretical prediction. The motivation behind our work was to understand the driving force behind this transition and to investigate whether the stretching penalty of the majority block is indeed the cause for the symmetry transition.

*Corresponding author. E-mail: edkramer@mrl.ucsb.edu.

 Published on Web 01/28/2010

Our approach is to blend a small amount of short majority block homopolymer (hPS) with the diblock copolymer and to compare the equilibrium structure in these films with that of the neat block copolymer. It has been suggested that thermal fluctuations can dislodge some of the minority block from their domains, and these chains can relieve the packing frustration of the close-packed structure and stabilize it.[2,18,20] In the self-consistent mean-field phase diagram, for highly asymmetric chains, a close-packed sphere phase exists between the BCC phase and the disordered phase.[2,19] The close-packed phase has not been observed in the bulk, except under the influence of an external field or in solution,[21] presumably because fluctuation effects that are not accounted for in mean-field theory stabilize the disordered phase. Nevertheless we expect that small weight fractions of a short majority block homopolymer could produce a similar effect as dislodged chains, without leading to a disordered phase.

The critical number of layers at which the transition from HCP to FCO occurs (n^*) can be estimated by eq 1[22]

$$n^* = 1 + \frac{f_l(\mathrm{BCC}) - f_l(\mathrm{HCP})}{f_b(\mathrm{HCP}) - f_b(\mathrm{BCC})} = 1 + \frac{\Delta_l}{\Delta_b} \quad (1)$$

where f_l is the free energy per chain of a monolayer and f_b is the free energy per chain in the bulk phase, $f_b(\mathrm{BCC}) < f_b(\mathrm{HCP})$ and $f_l(\mathrm{BCC}) > f_l(\mathrm{HCP})$. The homopolymer addition is expected to lower the entropic component of the free energy as the homopolymer can migrate to the highly stretched interstices and relieve the energetic penalty of stretching of the majority block. If the HCP is the more stretched phase, the homopolymer should cause a larger decrease in the free energy per chain of the HCP arrangement compared to the BCC. This would cause an increase in Δ_l and a decrease in Δ_b, hence leading to an increase in n^*.

While some theoretical studies of block copolymer−homopolymer blends have proposed that addition of homopolymer can stabilize frustrated morphologies, they have mostly focused on bulk systems and where the homopolymer size is comparable with the block copolymer[18,23] or when large volume fractions of the homopolymer are added.[24] Our studies extend these findings by focusing on asymmetric diblock copolymers in thin film geometry and studying the effect of addition of a small amount of short majority block homopolymer. The aim of these experiments is to develop insight into the role of entropic contributions to equilibrium geometry of thin films. This study also reveals a novel technique for expanding the window of close-packed spheres and other frustrated structures. To the best of our knowledge, this is the first experimental test of the prediction that the greater packing frustration of the HCP lattice relative to the BCC geometry is the reason why it is disfavored in bulk.

Experimental Procedure

The polymer used in these studies, spherical morphology poly(styrene-*b*-2-vinylpyridine), was synthesized by sequential anionic polymerization (M_n = 65 000 g/mol, N = 626, f_{P2VP} = 0.12, PDI = 1.04). We chose a polystyrene homopolymer (hPS) with M_n = 13 000 g/mol. This hPS is expected to be soluble in the PS matrix and have a relatively high diffusion coefficient.[24,25] Multilayer films were prepared on silicon substrates by spin-casting from dilute solutions of PS−P2VP and hPS in toluene. Three homopolymer weight fractions were studied: 4.75, 8, and 12 wt %. The films were heated to above the bulk order disorder temperature of the neat block copolymer (250 ± 7 °C or $\chi N_{ODT} \sim 54$) to fully disorder the lattice and then very slowly cooled to the annealing temperature (200 °C or $\chi N \sim 62$) and held for 1.5 days. This results in spherical microdomains of the P2VP block arranged in a well-ordered lattice with layering parallel to the substrate. The sphere radius is 5 nm with the close-packed rows separated by 22 nm. The difference in surface energies of the PS and P2VP species causes the P2VP block to preferentially wet the native oxide forming a brush layer of thickness about 18 nm and the PS block to wet the film−air interface. A Physical Electronics 6650 dynamic secondary ion mass spectrometer (SIMS) was used to identify the number of sphere layers in each film by tracking the CN^- signal, which is unique to P2VP. Film thickness was measured by X-ray reflectivity using a Pananalytical XRD Pro thin film diffractometer. Transmission electron microscopy (TEM) was used to investigate the 3D structure of the film with a FEI Tecnai G20 microscope operating at 200 kV. For TEM measurements, the films were annealed on a silicon substrate with a thick layer of silicon oxide. By immersing the substrate in an HF bath, the oxide was etched away releasing the polymer film which was then picked up on a TEM grid. Prior to imaging, the films were stained with iodine for 4 h to enhance electron scattering by the P2VP domains to obtain better contrast in the bright field images.

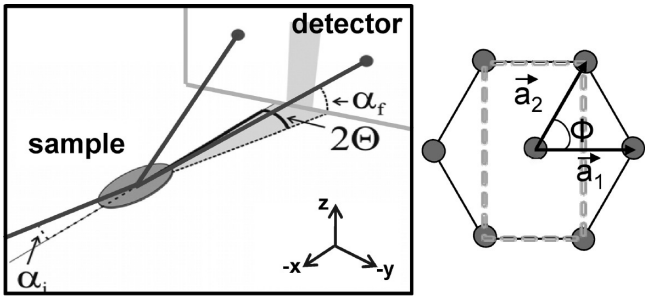

Figure 1. Left: schematic of the GISAXS setup. The X-ray beam is incident on the sample at an angle α_i. A detector records the intensity of the scattered wave in terms of the in-plane scattering angle 2θ and the out-of-plane scattering angle α_f Right: a general basis for in-plane packing.

For statistically representative structural data averaged over large areas, grazing incidence small-angle X-ray scattering (GISAXS) was used.[1,26−28] In the GISAXS geometry, the X-ray beam impinges the sample at a very small angle, giving rise to an elongated footprint (~1.5 cm) that results in intense scattering even from very thin films when a high-intensity synchrotron X-ray source is used. GISAXS is suited for our studies as it is a powerful tool for studying morphologies at the mesoscale, being sensitive to even minor lattice variations. GISAXS experiments were carried out at the Sector 8-IDE beamline at the Advanced Photon Source at Argonne National Laboratory. A transmission diamond monochromator provided intense radiation of wavelength of 0.1686 nm, and the scattered intensity was recorded by a MAR-2 CCD area detector and stored as a 2048 × 2048 16-bit tiff image. A lead beam stop was used to block the specular beam. The resulting data set was converted to a map of intensity $I(2\theta,\alpha_f)$, where 2θ is the in-plane diffraction angle and α_f is the out-of-plane diffraction angle (shown in Figure 1). Depth profiling of the structure of the films was carried out by controlling the penetration depth of the X-rays by varying the incident angle of the beam from below the critical angle of the polymer up to the critical angle of the substrate ($\alpha_{c,p} \approx 0.14°$, $\alpha_{c,s} \approx 0.24°$). Five 2D diffraction patterns were taken at each incident angle while moving the sample 0.1 mm horizontally before each measurement to prevent beam damage to the sample. Data from both sides of the beam stop were collected and were corrected for possible drift of the beam center. To assign an in-plane symmetry to the films, line integrations of intensity at low values of α_f were obtained and plotted against $q_{\|}$ and the peak positions were fit using a general in-plane basis having the following form:

$$a_1 = (a_1 \sin\phi,\ a_1 \cos\phi,\ 0) \quad (2)$$

$$a_2 = (0, a_2, 0) \quad (3)$$

Here a_2 is the nearest-neighbor spacing, a_1 is the next-nearest neighbor, and ϕ is the angle between the two. For HEX, $a_2 = a_1$

and $\phi = 60°$, while for orthorhombic symmetry a_1 and a_2 are unequal and $\phi < 60°$. The in-plane scattering vector from the (h,k) plane was written in terms of reciprocal space lattice vectors $\vec{b}_1$ and $\vec{b}_2$ as $q(h,k) = h\vec{b}_1 + k\vec{b}_2$. By fitting the peak positions in the experimental line profiles to obtain the values of a_1, a_2, and ϕ, it was ascertained whether the in-plane arrangement was hexagonal or orthorhombic.

While the in-plane symmetry can be assigned by the technique outlined above, there is no straightforward way to reconstruct the stacking of layers from the experimental GISAXS data due to contribution from scattering from the reflected beam. As the penetration depth of the X-rays above the critical angle of the polymer is more than the thickness of our samples, the transmitted beam can also be reflected by the substrate, which leads to multiple possibilities for scattering events.[1,29] However, there is an indirect approach to reconstruct the stacking from both GISAXS and TEM measurements. In the GISAXS approach, a structure model of the sample is assumed and the diffraction pattern is simulated, which is then compared with the experimental image to find a match. In our case, the in-plane arrangement was first determined by fitting the diffraction peak positions to eqs 2 and 3. The diffracted intensity was then simulated assuming different stacking arrangements (A−B−A type and A−B−C type). For simulating the scattered intensity, the kinematical scattering theory,[30,31] which assumes that an X-ray photon can be scattered only once, is no longer valid. Although dynamic scattering theory[30,32] takes multiple scattering effects into account, it is mathematically complex and suited only for simple systems. We used a simplified treatment called the distorted wave Born approximation (DWBA), which has been extensively used to analyze data from grazing incidence techniques on thin films.[1,26−28,33,34] By assuming that the scattered intensity is small compared to the incident intensity, we treated the scattering centers (the P2VP spheres) as perturbations in a homogeneous matrix. The unperturbed system (the uniform film) is treated using dynamic theory, while scattering from the perturbation is treated kinematically (assuming that the density of the scatterers is too small for them to scatter more than once). The formalism and techniques used here are similar to the those discussed in a previous paper by Stein et al.[1] The different homopolymer percentages were represented by varying the scattering length densities of the homogeneous matrix. The second approach was to image the films at different tilts using TEM, which gave us a projection of the lattice structure of the sample. Micrographs taken at tilts of 32° and 35° were visually compared with calculated projections of FCO and HCP lattices at those angles.

Self-Consistent-Field Theory Simulations

We have postulated that the addition of hPS can stabilize the HCP lattice by migrating to the highly stretched interstices of the HCP unit cell, which would reduce the entropic stretching penalty of the HCP inner layers. In order to confirm that the free energy "relief" brought about by the homopolymer is more for the HCP arrangement compared to the FCO symmetry, we used self-consistent-field theory[4,35,36] to calculate the free energies of the HCP and FCO lattices and track the distribution of homopolymer in the film. Self-consistent-field theory has been extensively used to predict equilibrium behavior of polymer melts in the past[20,37,38] and has also been successfully adopted for thin films.[22,39−41] Similar to the approach adopted by Stein et al. to estimate n^* for the neat diblock system,[22] we used eq 1 to estimate n^* for different percentages of homopolymer using the free energies obtained by SCFT calculations. Because of the approximations involved in eq 1 and the SCFT treatment, the value of n^* estimated by this approach is qualitative; however, it captures the driving force (namely Δ_1/Δ_b) for the symmetry transition. As the formalism adopted here is similar to that by Bosse et al.[42] and Cochran et al.,[3] we outline the salient features here, but for complete details the reader is referred to those publications. We utilized a "masking" technique detailed in an earlier paper[39] to confine the polymer to a thin film bound by planar interfaces by imposing a "wall" density field $\rho_w(\mathbf{r})$ that expels the polymer from the interfaces. This approach is similar to that employed by Matsen for thin film studies.[40] In the notation followed here, the diblock is referred to as AB, where B is the majority block. The homopolymer and wall are denoted by subscripts "hB" and "w", respectively. The melt incompressibility condition takes the form

$$\hat{\rho}_A + \hat{\rho}_B + \hat{\rho}_{hB} + \rho_w = \rho_0 \tag{4}$$

where $\hat{\rho}$ represents the number densities of the various components, and ρ_0 is the average total segment density. This constraint limits the polymer to be confined as a thin film in the normal direction. In the canonical ensemble, the partition function can be written as functional integrals over all polymer space curves

$$Z = \int \prod_{k=1}^{n_d} \mathscr{D}r_k \prod_{l=1}^{n_{hB}} \mathscr{D}r_{hB,l}[\delta(\hat{\rho}_A + \hat{\rho}_B + \hat{\rho}_{hB} + \rho_w - \rho_0)] \exp(-U_0[\{r_k, r_{hB,l}\}] - U_I[\{r_k, r_{hB,l}\}]) \tag{5}$$

where n_d and n_{hB} are the number of chains for the diblock and the homopolymer, respectively, and r_k and $r_{hB,l}$ are the space curves denoting the configuration of the kth Gaussian chain of a copolymer and the lth homopolymer chain, respectively. U_0 and U_I are the harmonic stretching energy of the Gaussian chain and the segment interaction energy, respectively, given by

$$U_0[r_k, r_{hB,l}] = \frac{1}{4R_g^2}\left(\sum_{k=1}^{n_d}\int_0^1 ds\left|\frac{dr_k(s)}{ds}\right|^2 + \sum_{l=1}^{n_{hB}}\int_0^{N_{hB}/N} ds\left|\frac{dr_{hB,l}(s)}{ds}\right|^2\right) \tag{6}$$

$$U_I[r_k, r_{hB,l}] = \frac{1}{\rho_0}\int_V d\mathbf{r}\,[\chi\hat{\rho}_A(\mathbf{r})(\hat{\rho}_B(\mathbf{r}) + \hat{\rho}_{hB}(\mathbf{r})) + \chi_{WA}\rho_W(\mathbf{r})\hat{\rho}_A(\mathbf{r}) + \chi_{WB}\rho_W(\mathbf{r})(\hat{\rho}_B(\mathbf{r}) + \hat{\rho}_{hB}(\mathbf{r}))] \tag{7}$$

Here χ, χ_{WA}, and χ_{WB} are the Flory-type segment−segment and segment−wall interaction parameters, respectively. R_g is the unperturbed radius of gyration of the diblock, and V is the system volume. Upon transformation of this model to a field theoretic form, the relevant energy functional (Hamiltonian) can be written as

$$H[W_+, W_-] = C\int_V d\mathbf{x}\left[\frac{1}{\chi N}W_-^2(\mathbf{x}) - \iota\phi(\mathbf{x})W_+(\mathbf{x}) - \frac{2\chi_w N}{\chi N}\phi_w(\mathbf{x})W_-(\mathbf{x})\right] - C(1-\phi_{hB})\overline{\phi}V\ln Q[\iota W_+ + W_-, \iota W_+ - W_-] - C\frac{\phi_{hB}\overline{\phi}V}{\alpha}\ln Q_{hb}[\iota W_+ - W_-] \tag{8}$$

where $C = \rho_0 R_g^3/N$, $\mathbf{x} = \mathbf{r}/R_g$, W_- is the exchange potential field, and W_+ is the pressure-like potential field. $\phi(\mathbf{x}) = \rho(\mathbf{x})/\rho_0$ is the total polymer volume fraction, and $\overline{\phi}$ is its spatial average, ϕ_{hB} is the homopolymer volume fraction, while $\phi_w = \rho_w(\mathbf{x})/\rho_0$ is the normalized wall density. Q and Q_{hB} stand for the single chain partition function for the diblock and homopolymer, respectively, and α is N_{hB}/N. The Hamiltonian was analyzed for saddle points in the mean-field limit of the above field theory. All the

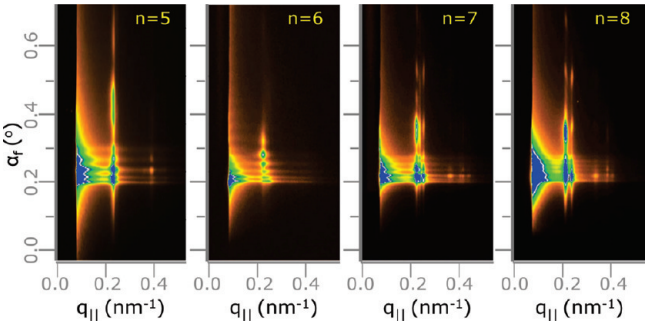

Figure 2. GISAXS intensity patterns $I(2\theta,\alpha_f)$ at incident angle α_i = 0.19° for films containing 8% hPS: (a) hexagonal symmetry in 5-layer film; (b) lack of higher order peaks in 6-layer film; (c) coexistence of the HEX and FCO structures in a 7-layer film; (d) FCO structure in 8-layer films.

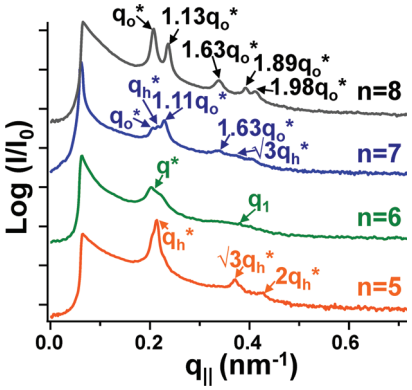

Figure 3. Variation of intensity with $q_{||}$ for 5-, 6-, 7-, and 8-layer films containing 8% hPS. The locations of the Bragg peaks show change in the in-plane symmetry from HEX to FCO as the film thickness is increased. The subscripts "h" and "o" refer to the HEX and FCO lattice, respectively.

fields were sampled on a discretized domain in three dimensions with a spatial resolution of at least $0.125R_g$ in the x, y, and z direction and were seeded with a plane wave basis. For calculating the bulk phase behavior, we carried out 3D unit cell calculations where the dimensions of unit cell were relaxed using an explicit scheme to minimize the local microscopic stress. A monolayer geometry was obtained by imposing a masked area in the normal direction. The unit cell parameters in the plane of the film were relaxed to minimize stress, while the out-of-plane lattice parameter was fixed by specifying the film thickness. The optimum film thickness was determined up to an accuracy of $0.2R_g$ by searching for the film thickness that minimized the surface tension as described elsewhere.[39] Periodic boundary conditions were imposed in the lateral direction. A prespecified smooth tanh function was used for the wall density profile.[39] This predetermined wall density enabled us to simulate an arbitrary type of confinement geometry and also include any type of surface−monomer interactions through choice of suitable wall interaction parameters. For the normal direction, symmetric boundary conditions were adopted by assuming that the walls had a common affinity for the majority block. The pseudospectral operator splitting algorithm,[43,44] known to have second-order accuracy in the chain contour step size and readily implemented using fast Fourier transforms, was used with a step size of 0.01 to solve the modified diffusion equation. A semi-implicit Seidel (SIS) field relaxation scheme[45] was used to update the field configurations. Iterations were carried out until the magnitude of the forces arising from the pressure and exchange chemical potential fields were below $10^{-5}k_BT$ per chain.

Results and Discussion

Structure Assignment. We will denote n^* as the lowest number of layers at which the equilibrium structure of the domains is FCO. For the neat copolymer films, $n^* = 5$.[1] GISAXS intensity patterns for films containing 8% hPS clearly show a transition in the diffraction pattern as the film thickness is increased (Figure 2). At $n = 5$, line integration evaluated at low values of α_f to extract the $I(q_{II})$ profile shows peaks at ratios of $1:\sqrt{3}:2$, which is characteristic of in-plane HEX arrangement (Figure 3). At $n = n^* = 8$ and beyond, we see the split first order peaks characteristic of two lattice vectors of unequal length in the in-plane structure, which implies that the symmetry of the films is FCO. There is a transition regime for $n < n^*$ ($n = 6$ and $n = 7$ in Figure 2) where coexistence between HEX and FCO symmetry is observed at this relatively short annealing time, indicating that the free energies of the two symmetries are comparable at these thicknesses. The second-order peaks at $n = 6$ for the blend films are weak while the first-order peak appears to be an overlap of two peaks, indicating lack of well-defined large grains. These results are similar to the results of Stein et al. for the neat block copolymer system, where they observed coexistence of HCP and FCO at $n = 4$ for similar annealing times. At longer annealing times in that neat copolymer case it became clear that HCP was the equilibrium phase at $n = 4$. With increasing thickness beyond n^*, the ratio of the peak positions approaches that of the BCC (110) structure ($1:\sqrt{4}/_3:\sqrt{8}/_3$). As the penetration depth of X-rays can be controlled by varying the incident angle,[46] profiling of the structure at different depths was carried out by varying the incident angle from below the critical angle of the polymer up to the critical angle of the substrate ($\alpha_{c,p} \approx 0.14°$, $\alpha_{c,s} \approx 0.24°$) to ensure that surface reconstruction was not occurring. For all the films under study it was confirmed that there was no difference in the in-plane arrangement at different depths, thus confirming that the added homopolymer has stabilized the unfavorable HEX arrangement for the internal layers.

The TEM results are in excellent agreement with the GISAXS data. The micrographs of Figure 4 correspond to samples whose GISAXS profiles are shown in Figure 3. These TEM micrographs clearly show that a well-ordered HCP arrangement transitions to a structure with FCO in-plane symmetry as the number of sphere layers is increased. For films that had very broad second-order peaks in the scattering profiles ($n = 6$ in Figures 2 and 3), TEM images showed coexistence of several small randomly oriented grains of both FCO and HCP morphologies. This is consistent with the theory of kinematical scattering, which states that X-ray diffraction peaks broaden either when crystallites become smaller than about a micrometer or if lattice defects are present in large enough abundance.[31] However, with the exception of these transition thicknesses, TEM micrographs show dramatically improved grain size (~10 μm^2) and ordering compared to the films of neat copolymer (< 2 μm^2).[1] This is a very large defect-free grain size for a block copolymer film without any sort of imposed field or physical or chemical patterning. The blended homopolymer probably makes the kinetics of grain coarsening more facile, which results in the improved ordering. Although it has been suggested that low molecular weight homopolymers tend to disorder a microstructure[23] similar to a neutral solvent by reducing χ,[47] we find that by limiting the homopolymer to small weight fractions we inhibit its tendency to distribute uniformly.

Simulation of scattering using the DWBA framework[1,33,28,27] assuming A−B−A stacking for the multilayer films showed excellent agreement with the experimental intensity maps

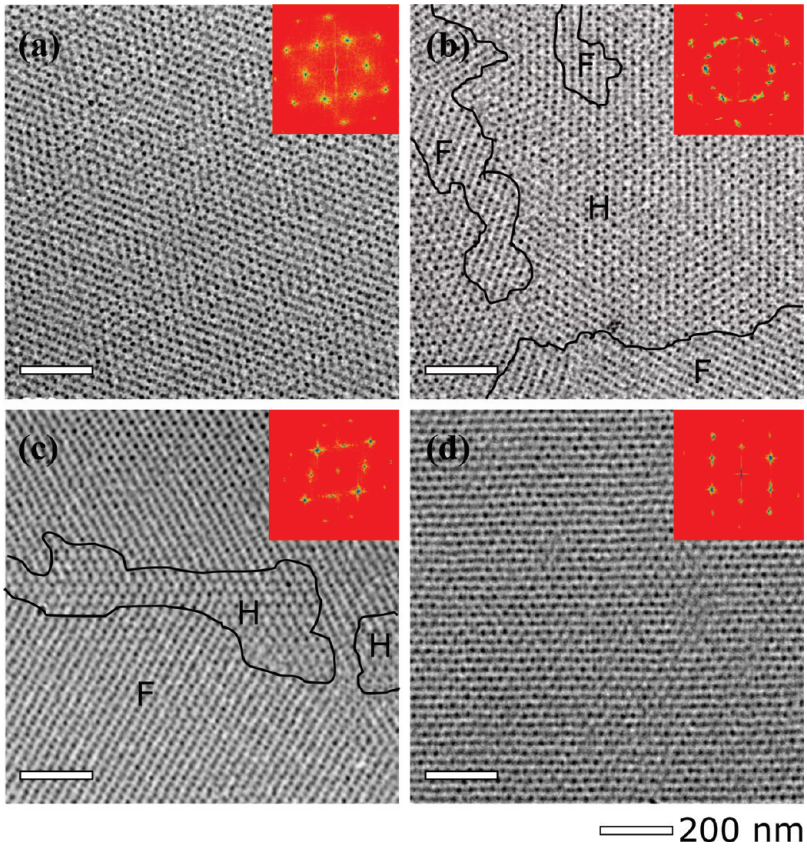

Figure 4. TEM micrographs for hPS = 8%. (a) $n = 5$: HCP symmetry; (b) $n = 6$: small grains of both FCO and HCP symmetries; (c) $n = 7$: large grains of FCO interspersed with grains of HCP; (d) $n = 8$: very well ordered grains of FCO packing (grain size ~20 μm^2) are observed. Inset: Fourier transform of the image.

(Figure 5). Prominent features such as the position of the diffraction peaks at that incident angle and peaks due to electric field enhancement were matched, which ensured that the lattice parameters, film thickness, and space groups were correct. TEM micrographs at different tilts also corroborated the space group assignment (Figure 6).

From the GISAXS and TEM data, we can conclude that $n^* = 6$ for films containing 4.75% homopolymer, $n^* = 8$ when the homopolymer addition was increased to 8%, and $n^* = 9$ for 12 wt %. Hence, n^* increases continuously with an increase in the percentage of homopolymer added (Figure 7). However, we expect that this increase can occur only up to a limit, until the majority block chains are completely relaxed, beyond which matrix swelling and micelle movement may be expected to occur. It is also interesting to note that in Figure 7 the region of coexistence in thickness grows wider for increased vol % of hPS. One possible explanation for this may be that the blend is a two-component system and therefore there can be true coexistence of two phases with different hPS compositions. For example, more hPS may dissolve in the HEX phase than in the FCO phase at equilibrium.

Self-Consistent-Field Theory Simulation Results. Using self-consistent-field theory, the free energy per chain for HEX and BCC arrangement of spheres for films containing different homopolymer percentages was estimated. While the addition of the homopolymer is expected to lower the free energy by relieving the packing frustration, the swelling of the block copolymer corona by the homopolymer may increase the stretching energy. However, the SCFT simulations show that addition of low weight fractions of homopolymer lowers the net free energy per chain in monolayer

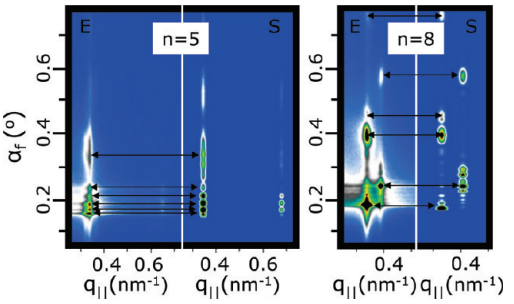

Figure 5. Strong agreement between simulated scattering (S) assuming ABA stacking and experimental out-of-plane GISAXS intensity patterns (E) for films containing 8% homopolymer. Left: HCP lattice at $n = 5$. Right: FCO symmetry at $n = 8$ layers.

and bulk geometries for both HEX and BCC symmetries as compared to the neat case. The free energy difference between the two symmetries is changed by addition of the homopolymer, which alters their relative stabilities. The estimated value of n^* for homopolymer percentages ranging from 0 to 11% is shown in Figure 8. The masking method used for imposing the monolayer geometry generally limits convergence due to the large pressure field values induced near the wall−polymer interfaces; thus, the free energy value of the monolayer was found to be sensitive to the initial seeded configuration. Because of this, we had to accelerate the search over the configurational space by seeding the simulation with various initial conditions. The simulations reveal that n^* increases continuously with increasing hPS percentage for low volume fractions of the homopolymer, which is consistent with our experimental observations. The

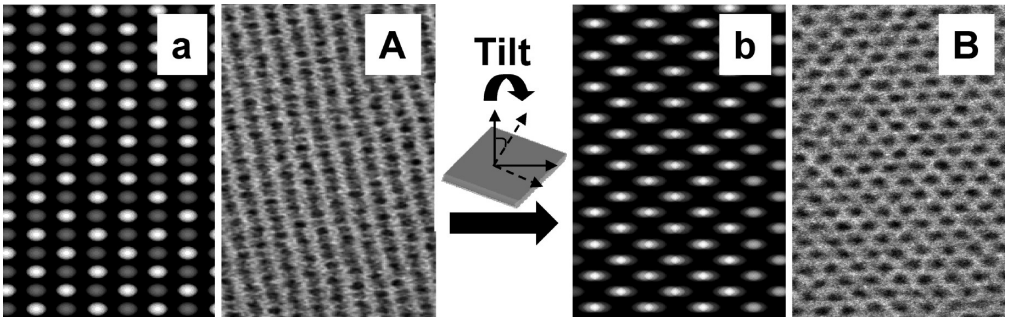

Figure 6. Confirmation of stacking by imaging a 9-layer film containing 8% hPS at 0° (LHS) and 30° (RHS) tilt angles and comparing with simulations. (a) and (b) are simulated images of an FCO lattice with ABA stacking and (A) and (B) are the corresponding TEM micrographs taken at the same angles.

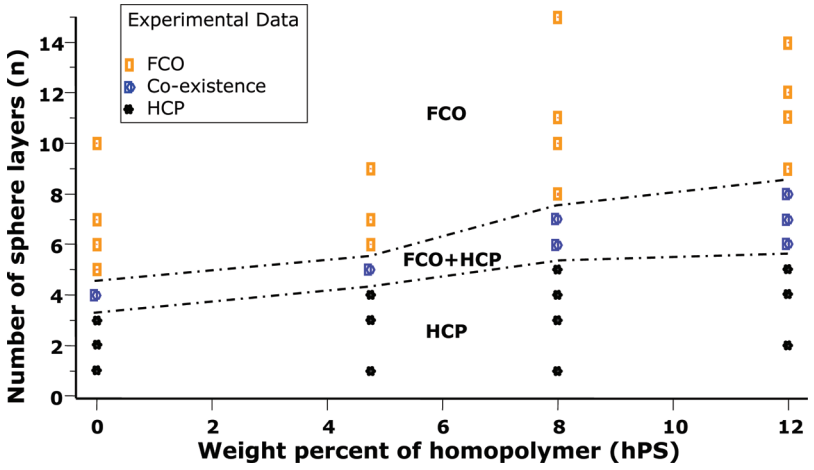

Figure 7. Experimental phase diagram for the different homopolymer percentages studied showing expansion of the window for close-packed spheres by addition of homopolymer.

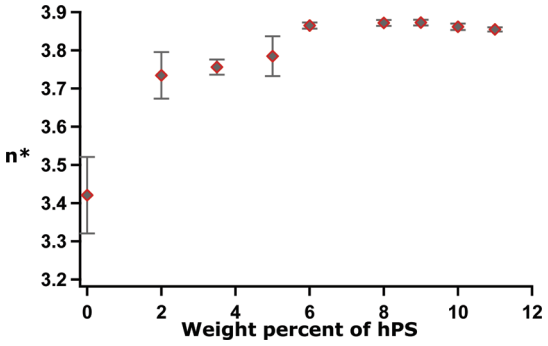

Figure 8. n^* for different homopolymer percentages, using free energy values calculated by SCFT.

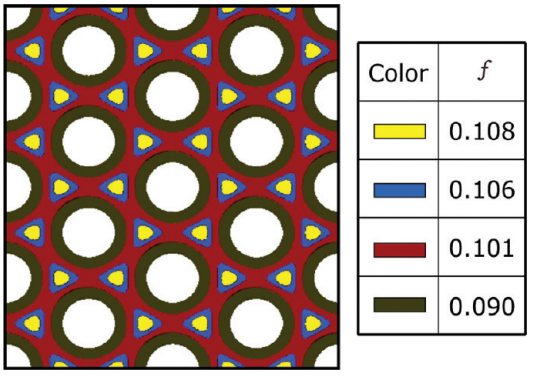

Figure 9. Top view of the unit cell for a film containing 8% hPS, showing the distribution of the homopolymer at $\chi N = 72$. Isosurfaces demarcating the areas corresponding to certain volume fractions of the homopolymer have been shown. The figure shows that the homopolymer is concentrated at the interstices that would otherwise have to be filled by highly stretched majority block chains.

increase in the calculated n^* is smaller than that observed experimentally, however. Because of approximations both in the eq 1 and in the SCFT treatment, and the sensitivity of n^* to the error in the estimated free energy, the value of n^* is not expected to be quantitative. The n^* values reported in Figure 8 were obtained using the minimum free energies per chain f_1 from the limited set of initial configurations we studied, while the error bars refer to the deviation from the average value. While a more exact estimate may be obtained by computationally expensive SCFT simulations for multilayer films or by sampling several other initial configurations, this semiphenomenological treatment is sufficient for obtaining a qualitative guide to the behavior of the real system.

The distribution of homopolymer as calculated by self-consistent mean-field theory for a unit cell of a monolayer film with HEX symmetry is shown in Figure 9. It is clearly seen that the homopolymer is concentrated at the interstices of the Wigner−Seitz cell where the majority block would have to stretch the most. The concentration of the homopolymer decreases away from the interstices.

Comparison between the majority block arrangement in the neat and blend films shown in Figure 10 shows the relaxation brought about by addition of the homopolymer. The homopolymer preferentially migrates to the regions which would otherwise have to be filled by highly

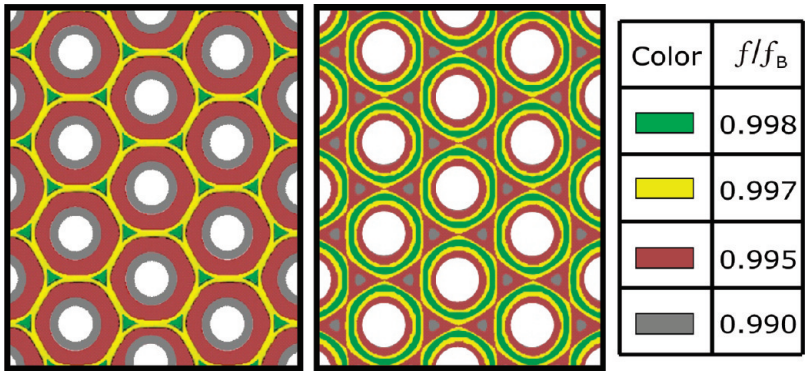

Figure 10. Comparison of distribution of the majority block in neat films (left) and blend films (right). The local volume fraction f is normalized by its maximum value in the matrix f_B. Note that the maximum concentration of the majority block (color coded by green) in the neat case is at the interstices of the Wigner−Seitz cell, while in the blend case it is arranged in a more relaxed manner, with less localization at the interstices. Images shown are top views of the respective unit cells.

stretched majority block chains and allows the majority block to relax to a state with more uniform curvature. The packing frustration of the lattice is reduced as the chains are no longer required to stretch unequally to reach the interstices. This lowers the free energy penalty of the hexagonal arrangement significantly and makes it the favored arrangement for an increased number of layers as compared to the neat state.

Conclusion

Self-assembly of block copolymers in thin films can yield templates for nanolithographic patterning of substrates on very small length scales as well as ordered multilayer structures for membrane and electronic applications. On a fundamental level these thin block copolymer films raise many interesting questions about self-assembly in 2D and how the transition from 2D to 3D occurs as the film is increased in thickness. We have highlighted one such set of questions, how the packing of spherical block copolymer domains confined to a thin film changes as the thickness of the film is increased layer by layer of spheres, with small weight fraction additions of low molecular weight homopolymer that can fill interstices between spheres. In multilayer thin films of spherical morphology block copolymers, the surface layers prefer hexagonal symmetry while the inner layers prefer BCC. Competition between the preferred arrangement for the internal layers versus that of the surface layers leads to a symmetry transition in films of spherical morphology PS−P2VP as the film thickness is increased. We have shown that addition of majority block homopolymer can stabilize the HCP arrangement to an increased number of layers. SCFT simulations are in good agreement with the experimental trend and also show that the homopolymer is preferentially segregated at the interstices of the unit cell. As the interstices are the regions where the majority block needs to stretch the most, this shows that the effect of adding the homopolymer is to reduce the amount of stretching of the polymer majority block in the matrix. Since this leads to a stabilization of the HCP phase, it strongly suggests that the excessive stretching penalty of the HCP arrangement was the reason for its destabilization, which is consistent with SCFT predictions. Besides gaining a better understanding of the physics of multilayer films, this study is also technologically relevant as it shows that homopolymer can be used to stabilize frustrated morphologies in thin films, improve grain size by speeding up grain coarsening, and suppress undesirable thickness-dependent symmetry transitions.

Acknowledgment. We gratefully acknowledge funding from NSF DMR Polymer program Contract No. DMR-0307233 and CSP Technologies Fellowship for support of V.M. S.H. and G.H.F. derived partial support from NSF Grant No. DMR-0904499 and the MARCO center on Functional Engineered NanoArchitectonics (FENA). Use of the MRL Facilities was supported by the MRSEC Program of the National Science Foundation under Contract No. DMR-0520415. Use of the APS was supported by the U.S. D.O.E. office of Basic Energy Sciences under Contract No. DE-AC02-06CH11357.

References and Notes

(1) Stein, G. E.; Kramer, E. J.; Li, X. F.; Wang, J. *Macromolecules* **2007**, *40*, 2453–2460.
(2) Matsen, M. W.; Bates, F. S. *Macromolecules* **1996**, *29*, 1091–1098.
(3) Cochran, E. W.; Garcia-Cervera, C. J.; Fredrickson, G. H. *Macromolecules* **2006**, *39*, 2449–2451.
(4) Helfand, E.; Tagami, Y. *J. Chem. Phys.* **1972**, *56*, 3592–&.
(5) Bates, F. S.; Fredrickson, G. H. *Annu. Rev. Phys. Chem.* **1990**, *41*, 525–557.
(6) Bates, F. S.; Schulz, M. F.; Khandpur, A. K.; Förster, S.; Rosedale, J. H.; Almdal, K.; Mortensen, K. *Faraday Discuss.* **1994**, *98*, 7–18.
(7) Förster, S.; Khandpur, A. K.; Zhao, J.; Bates, F. S.; Hamley, I. W.; Ryan, A. J.; Bras, W. *Macromolecules* **1994**, *27*, 6922–6935.
(8) Kim, H. C.; Jia, X. Q.; Stafford, C. M.; Kim, D. H.; McCarthy, T. J.; Tuominen, M.; Hawker, C. J.; Russell, T. P. *Adv. Mater.* **2001**, *13*, 795.
(9) Segalman, R. A.; Yokoyama, H.; Kramer, E. J. *Adv. Mater.* **2001**, *13*, 1152–1155.
(10) Park, M.; Harrison, C.; Chaikin, P. M.; Register, R. A.; Adamson, D. H. *Science* **1997**, *276*, 1401–1404.
(11) Kersting, R. E. *Synthetic Polymer Membrane*; Wiley: New York, 1985.
(12) Widawski, G.; Rawiso, M.; Francois, B. *Nature* **1994**, *369*, 387–389.
(13) Lambooy, P.; Russell, T. P.; Kellogg, G. J.; Mayes, A. M.; Gallagher, P. D.; Satija, S. K. *Phys. Rev. Lett.* **1994**, *72*, 2899–2902.
(14) Koneripalli, N.; Singh, N.; Levicky, R.; Bates, F. S.; Gallagher, P. D.; Satija, S. K. *Macromolecules* **1995**, *28*, 2897–2904.
(15) Knoll, A.; Tsarkova, L.; Krausch, G. *Nano Lett.* **2007**, *7*, 843–846.
(16) Thomas, E. L.; Kinning, D. J.; Alward, D. B.; Henkee, C. S. *Macromolecules* **1987**, *20*, 2934–2939.
(17) Gruner, S. M. *J. Phys. Chem.* **1989**, *93*, 7562–7570.
(18) Matsen, M. W. *Macromolecules* **1995**, *28*, 5765–5773.
(19) Semenov, A. N. *Macromolecules* **1989**, *22*, 2849–2851.
(20) Matsen, M. W. *J. Phys.: Condens. Matter* **2002**, *14*, R21–R47.
(21) Hamley, I. W.; Mai, S. M.; Ryan, A. J.; Fairclough, J. P. A.; Booth, C. *Phys. Chem. Chem. Phys.* **2001**, *3*, 2972–2980.
(22) Stein, G. E.; Cochran, E. W.; Katsov, K.; Fredrickson, G. H.; Kramer, E. J.; Li, X.; Wang, J. *Phys. Rev. Lett.* **2007**, 98.
(23) Whitmore, M. D.; Noolandi, J. *Macromolecules* **1985**, *18*, 2486–2497.
(24) Semenov, A. N. *Macromolecules* **1993**, *26*, 2273–2281.
(25) Green, P. F.; Russell, T. P.; Jerome, R.; Granville, M. *Macromolecules* **1988**, *21*, 3266–3273.
(26) Rauscher, M.; Salditt, T.; Spohn, H. *Phys. Rev. B* **1995**, *52*, 16855–16863.

(27) Holy, V.; Pietsch, U.; Baumbach, T. *High Resolution X-ray Scattering from Thin Films and Multilayers*; Springer Tracts in Modern Physics; Springer: Berlin, 1999.
(28) Lee, B.; Park, I.; Yoon, J.; Park, S.; Kim, J.; Kim, K. W.; Chang, T.; Ree, M. *Macromolecules* **2005**, *38*, 4311–4323.
(29) Chang, S. L. *X-Ray Multiple-Wave Diffraction*; Springer Series in Solid-State Sciences; Springer: Berlin, 2004; Vol. *143*.
(30) Azaroff, L. V.; Kaplow, R.; Kato, N.; Weiss, R. J.; Wilson, A. J. C.; Young, R. A. *X-Ray Diffraction*; McGraw-Hill: New York, 1974.
(31) Warren, B. E. *X-ray Diffraction*; Dover Publ.: New York, 1990.
(32) Authier, A. *Dynamical Theory of X-ray Diffraction*; Oxford University Press: New York, 2001.
(33) Sinha, S. K.; Sirota, E. B.; Garoff, S.; Stanley, H. B. *Phys. Rev. B* **1988**, *38*, 2297–2311.
(34) Renaud, G.; Lazzari, R.; Revenant, C.; Barbier, A.; Noblet, M.; Ulrich, O.; Leroy, F.; Jupille, J.; Borensztein, Y.; Henry, C. R.; Deville, J. P.; Scheurer, F.; Mane-Mane, J.; Fruchart, O. *Science* **2003**, *300*, 1416–1419.
(35) Helfand, E.; Sapse, A. M. *J. Chem. Phys.* **1975**, *62*, 1327–1331.
(36) de Gennes, P. G. *Scaling Concepts in Polymer Physics*; Cornell University Press: Ithaca, NY, 1979.
(37) Matsen, M. W.; Schick, M. *Phys. Rev. Lett.* **1994**, *72*, 2660–2663.
(38) Fredrickson, G. H. *The Equilibrium Theory of Inhomogenous Polymers*; Oxford University Press: New York, 2006.
(39) Khanna, V.; Cochran, E. W.; Hexemer, A.; Stein, G. E.; Fredrickson, G. H.; Kramer, E. J.; Li, X.; Wang, J.; Hahn, S. F. *Macromolecules* **2006**, *39*, 9346–9356.
(40) Matsen, M. W. *J. Chem. Phys.* **1997**, *106*, 7781–7791.
(41) Pickett, G. T.; Balazs, A. C. *Langmuir* **2001**, *17*, 5111–5117.
(42) Bosse, A. W.; Garcia-Cervera, C. J.; Fredrickson, G. H. *Macromolecules* **2007**, *40*, 9570–9581.
(43) Rasmussen, K. O.; Kalosakas, G. *J. Polym. Sci., Part B: Polym. Phys.* **2002**, *40*, 1777–1783.
(44) Tzeremes, G.; Rasmussen, K. O.; Lookman, T.; Saxena, A. *Phys. Rev. E* **2002**, *65*, 041806.
(45) Ceniceros, H. D.; Fredrickson, G. H. *Multiscale Model. Simul.* **2004**, *2*, 452.
(46) Lin, Y.; Boker, A.; He, J. B.; Sill, K.; Xiang, H. Q.; Abetz, C.; Li, X. F.; Wang, J.; Emrick, T.; Long, S.; Wang, Q.; Balazs, A.; Russell, T. P. *Nature* **2005**, *434*, 55–59.
(47) Fredrickson, G. H.; Leibler, L. *Macromolecules* **1989**, *22*, 1238–1250.